Effects of Cloud Parameterization on the Simulation of Climate Changes in the GISS GCM. Part II: Sea Surface Temperature and Cloud Feedbacks

MAO-SUNG YAO

SGT, Inc., NASA Goddard Space Flight Center, Institute for Space Studies, New York, New York

ANTHONY D. DEL GENIO

NASA Goddard Space Flight Center, Institute for Space Studies, New York, New York

(Manuscript received 21 December 2001, in final form 26 March 2002)

ABSTRACT

The influence of the sea surface temperature distribution on cloud feedbacks is studied by making two sets of doubled CO_2 experiments with the Goddard Institute for Space Studies (GISS) GCM at 4° latitude × 5° longitude resolution. One set uses Q fluxes obtained by prescribing observed sea surface temperatures (MODELII′), and the other set uses Q fluxes obtained by prescribing the simulated sea surface temperature of a coupled ocean–atmosphere model (MODELIIO). The global and annual mean surface air temperature change (ΔT_s) obtained in MODELII′ is reduced from 4.11° to 3.02°C in MODELIIO. This reduced sensitivity, aside from reduced sea ice/snow–albedo feedback, is mainly due to cloud feedback that becomes nearly neutral in MODELIIO. Furthermore, the negative effect on climate sensitivity of anvil clouds of large optical thickness identified by Yao and Del Genio changes its sign in MODELIIO primarily due to sharply reduced increases of cloud water in the tropical upper troposphere. Colder tropical sea surface temperature in MODELIIO results in weaker deep convective activity and a more humid lower atmosphere in the warmer climate relative to MODELII′, which then removes the negative feedback of anvil clouds and sharply reduces the positive feedback of low clouds. However, an overall positive cloud optical thickness feedback is still maintained in MODELIIO.

It is suggested that the atmospheric climate sensitivity, partially due to changes in cloud feedbacks, may be significantly different for climate changes associated with different patterns of sea surface temperature change, as for example in warm versus cold paleoclimate epochs. Likewise, the climate sensitivity in coupled atmosphere–ocean models is also likely to be significantly different from the results obtained in Q-flux models due to the different simulations of sea surface temperature patterns in each type of model.

1. Introduction

Cloud feedback is one of the major uncertainties in climate change problems. Depending on the treatments of moist convection and large-scale clouds in climate models, the cloud feedback appears to produce a threefold variation in one measure of global climate sensitivity (Cess et al. 1990).

While Cess et al. (1990, 1996) performed climate sensitivity experiments using many different general circulation models (GCMs) by increasing/decreasing sea surface temperature (SST) 2°C as a surrogate for a forced climate change, Mitchell et al. (1989) and Senior and Mitchell (1993) conducted four doubled CO_2 experiments using different cloud parameterizations with a single GCM. They found the presence or absence of cloud microphysical and optical thickness feedbacks can cause the global warming of the surface air temperature to range from 1.9° to 5.4°C. Likewise, Yao and Del Genio (1999) used the Goddard Institute for Space Studies (GISS) GCM to perform a set of doubled CO_2 experiments mainly to identify the effects of individual components of the moist convection and large-scale cloud parameterizations on cloud feedbacks, with a focus on the effects of convective anvil clouds and cloud optical thickness.

In Yao and Del Genio (1999), a mixed layer ocean model is applied using *Q* fluxes generated in integrations where observational sea surface temperatures were prescribed. However, it is a reasonable question to ask whether predicted cloud feedbacks would have the same sign and magnitude if the prescribed sea surface temperatures were to deviate significantly from observations, as is commonly the case in dynamic coupled ocean–atmosphere models (AOGCMs; cf. Mechoso et al. 1995) and in the real world in different paleoclimate epochs.

Rind (1998) estimated the effects of a change in the latitudinal sea surface temperature gradient on climate

Corresponding author address: Anthony D. Del Genio, NASA GISS, 2880 Broadway, New York, NY 10025.
E-mail: adelgenio@giss.nasa.gov

changes. It was estimated that low-latitude temperature gradients similar to today's may have occurred in the Mesozoic and in the Little Ice Age, while reduced gradients were more likely in the Pliocene, Eocene, Younger Dryas, and Last Glacial Maximum. The zonal variations, as well as the meridional variations, of surface temperature are also likely to have significant impact on the climate sensitivity (Senior and Mitchell 1993; Del Genio et al. 1996).

In the present study, we generate sea surface temperature boundary conditions by making a coupled ocean–atmosphere model run, which produces different meridional and zonal gradients of sea surface temperature from those observed. Then, by making an additional set of doubled CO_2 experiments using the Q fluxes obtained by prescribing the coupled model-generated sea surface temperatures, we can examine the effects of sea surface temperature patterns on the climate changes, with a focus on the cloud feedbacks.

We describe the model and experiments in section 2. We compare the results for the current climate in section 3. In section 4, we compare the climate changes resulting from doubling CO_2 and analyze the climate sensitivity and changes of cloud radiative forcing (CRF). Section 5 presents our discussion and conclusions.

2. The models and experiments

a. The models

Except for the parameterizations of large-scale clouds and moist convection we use a GCM version similar to the GISS Model II of Hansen et al. (1983). For the large-scale cloud parameterization, we use the prognostic scheme of Del Genio et al. (1996); for moist convection, we use the parameterization described in Del Genio and Yao (1993).

To parameterize large-scale cloud formation, Del Genio et al. (1996) follow the approach of Sundqvist et al. (1989). A grid box is divided into a cloudy part, of cloud fraction b, with relative humidity $\mathrm{RH}_s = 1$, and a clear part $(1 - b)$, where

$$b = (\mathrm{RH} - \mathrm{RH}_o)/(\mathrm{RH}_s - \mathrm{RH}_o), \quad (1)$$

where RH is the gridbox relative humidity, and $\mathrm{RH}_o = \mathrm{RH}_{oo} + b(\mathrm{RH}_s - \mathrm{RH}_{oo})$ is the clear-region relative humidity. The $\mathrm{RH}_{oo} = 0.6$ is the threshold relative humidity for large-scale clouds to form. A continuity equation for the cloud water content (m) is used, that includes the effect of condensation of water vapor, evaporation of cloud water and rainwater, the conversion of cloud water to precipitation, and the subgrid-scale dynamical source/sink of cloud water due to convective condensate detrainment and cloud-top entrainment instability. Then, the cloud visible optical thickness is calculated by

$$\tau = 3\mu\Delta Z/2\rho_w r_e, \quad (2)$$

where $\mu = m\rho/b$ is the cloud water density, ρ is the air density, ρ_w is the water density, ΔZ is the cloud physical thickness, and $r_e \cong 1.3 \times r$, the effective radius of the droplet size distribution (Hansen and Travis 1974), is proportional to the volume-weighted mean droplet radius r.

The parameterization of moist convection of Del Genio and Yao (1993) assesses instability based on the moist static energy of a parcel lifted one model layer and calculates the convective updraft mass and compensating environmental subsidence by requiring that neutral stability be restored at cloud base after the convection occurs (Yao and Del Genio 1989). The parameterization allows a fraction of the condensate obtained from the deep convection to detrain into the environment and form anvil clouds. The detrained condensate then combines with any anvil cloud water generated by large-scale cloud formation in the same grid box. The optical thickness of anvil clouds is predicted by (2), and the cloud cover of anvil clouds in the absence of large-scale clouds is $10C_m$, where C_m is the ratio of the convective mass to the gridbox air mass. The optical thickness for the nonanvil portion of convection is prescribed as in Hansen et al. (1983), and the cloud cover is C_m.

The only other difference in model physics relative to Model II is that the effect of sea ice puddling is crudely estimated (Hansen et al. 1997). When the ground temperature over sea ice is greater than -0.1°C, the sea ice albedo is set to 0.25 in the visible and 0.1 in the near-infrared (Model II uses 0.55 and 0.3, respectively). In the runs analyzed by Yao and Del Genio (1999), sea ice puddling was mistakenly activated at all temperatures. We repeat here several of their experiments with correct puddling now included to assess its effect. The correct sea ice puddling sharply increases the sea ice–albedo feedback, and thus the climate sensitivities reported in this paper are about 1°C higher than those in Yao and Del Genio (1999). However, the presence or absence of sea ice puddling has little effect on the cloud feedbacks on which we focus.

The dynamic ocean model to which we couple is one of the National Center for Atmospheric Research (NCAR) versions of the Geophysical Fluid Dynamics Laboratory (GFDL) ocean model (cf. Large et al. 1997), and was implemented at GISS without flux correction and with fixed sea ice. The model is initialized with the Levitus data (Levitus 1982), and is run with 25 layers and with zonal grid size of 3.6° longitude and meridional grid size decreasing from the midlatitudes (3.4° latitude) toward the equator and Poles (1.8° latitude). For simplicity, the coupled model does not allow partial land or ocean in a grid box, which may account for some differences in the sea surface temperature, particularly over islands and near coastal lines.

b. The experiments

Two sets of equilibrium doubled CO_2 experiments, three experiments in each set, were conducted using

TABLE 1. Comparison of physics and SST specifications for computing Q fluxes in the experiments.

	MODELII′	NOANVIL	NOTAUFB	MODELIIO	NOANVILO	NOTAUFBO
SST	Climatology	Climatology	Climatology	Coupled model	Coupled model	Coupled model
Cloud optical thickness	Predicted	Predicted	Fixed	Predicted	Predicted	Fixed
Anvil clouds	On	Off	On	On	Off	On

coupled atmosphere–mixed layer models, all run at 4° (latitude) × 5° (longitude) resolution and nine vertical layers. One set uses *Q* fluxes obtained from the local surface energy imbalance in preliminary 5-yr runs with observed sea surface temperatures and fixed sea ice as in Hansen et al. (1984); the other set uses *Q* fluxes obtained from the preliminary runs that used prescribed coupled model-generated sea surface temperatures that were calculated as the mean of the last 10 yr after 50 yr of simulation. Each experiment ran for 40 yr for both 1 (315 ppm) and 2 (630 ppm) × CO_2 concentration. The means of the last 10 yr are generally used in this report. But the cloud radiative forcing and radiative quantities (shown in Table 4) are means of the last 5 yr. While a 50-yr run is too short for an AOGCM run to reach equilibrium, it is probably adequate for our purpose of exploring the effect on clouds of different sea surface temperature patterns, since many AOGCMs (e.g., Russell et al. 1995) project future climate changes by initializing the model with the current state and do not run to final equilibrium state. Separate *Q*-flux distributions are calculated for each experiment. The current version of the GCM we use (MODELII′, discussed below) is close to planetary and surface energy balance, but several of the sensitivity experiments have significant global imbalance (see Table 2). To correct this, incoming solar radiation is modified at the ocean surface to remove this imbalance globally as in Hansen et al. (1984). The calculated *Q* fluxes are local deviations from the global mean energy balance. The experiments are described as follows:

1) MODELII′: Similar to GISS Model II of Hansen et al. (1983), but using the new parameterization of large-scale clouds and moist convection, and using *Q* fluxes that were obtained by prescribing the observed sea surface temperatures and sea ice.
2) NOANVIL: Similar to MODELII′, but without the anvil cloud parameterization. The detrained condensate is assumed to immediately precipitate to the

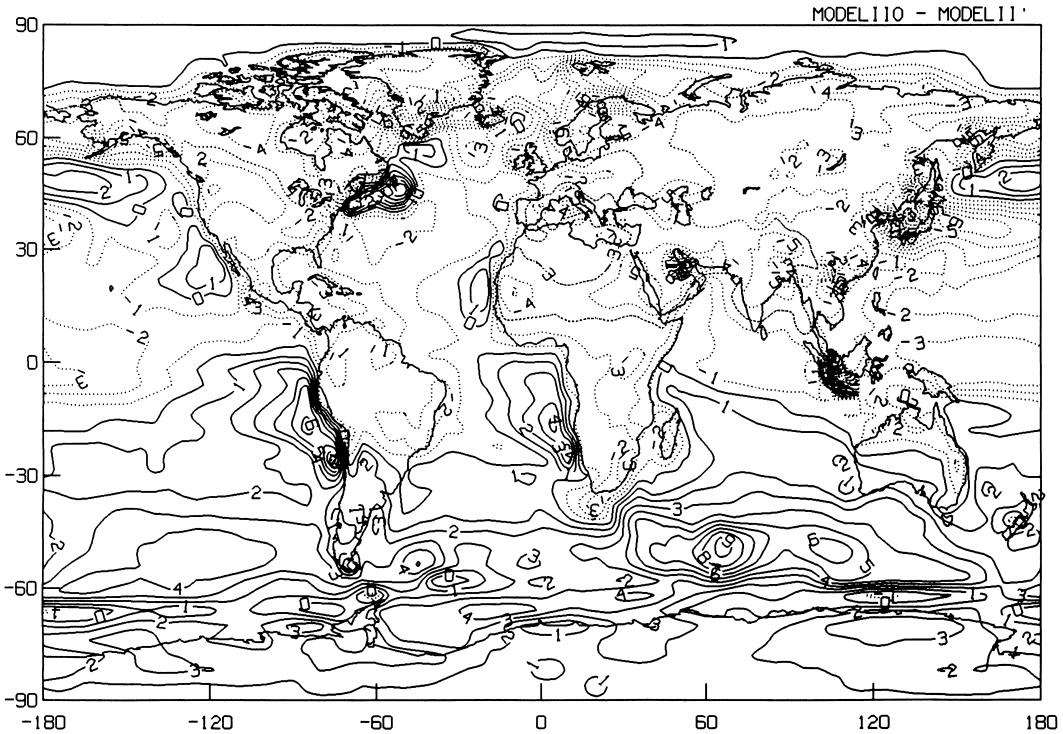

FIG. 1. Geographical distribution of annual mean ground temperature (°C) differences between MODELIIO and MODELII′.

TABLE 2. Selected global mean and annual mean climate parameters. Here Q is the absorbed solar radiation, and F is the net longwave radiation. TOA is top of atmosphere. Cloud cover and albedo are in %; radiative and turbulent fluxes are in W m^{-2}.

	MODELII′	NOANVIL	MODELIIO	NOANVILO
T_s (°C)	13.74	13.34	13.14	12.91
T_g (°C)	14.65	14.25	14.10	13.90
Total cloud	57.7	55.8	57.4	55.3
Low cloud	48.1	48.0	47.6	47.6
Middle cloud	16.4	11.7	16.5	11.5
High cloud	16.2	13.7	15.8	13.4
Planetary albedo	31.02	30.12	30.4	29.36
Ground albedo	12.11	12.25	11.43	11.41
Q at TOA	235.9	238.9	238.0	241.5
F at TOA	−235.8	−239.8	−234.4	−238.5
Net radiation at TOA	0.1	−0.9	3.6	3.0
Q at surface	169.4	172.2	171.7	175.0
F at surface	−45.7	−46.7	−46.7	−47.9
Net radiation at surface	123.6	125.6	125.0	127.0
Net heat at surface	−0.81	−2.03	2.84	2.05
TOA CRF (W m^{-2})	−37.98	−38.03	−36.98	−37.04
Shortwave CRF	−55.72	−52.08	−54.65	−51.02
Longwave CRF	17.74	14.05	17.67	13.98
Latent heat flux	−100.1	−103.1	−97.2	−100.1
Sensible heat flux	−23.2	−23.3	−23.9	−23.8
Precipitation (mm day^{-1})	3.47	3.57	3.37	3.46
Ocean ice (%)	5.0	5.6	4.4	4.4
Lapse rate (°C km^{-1})	5.99	6.0	6.12	6.15
Precipitable water (mm)	25.5	24.0	24.1	22.7

surface, with some evaporation as it falls, and cumulus cloud fraction is not increased by a factor of 10 in the upper troposphere.

3) NOTAUFB: Similar to MODELII′, but the cloud optical thickness is prescribed to be a fixed function of pressure only, as in Eq. (21) of Hansen et al. (1983).
4) MODELIIO: Similar to MODELII′, but using Q fluxes that were obtained by prescribing the coupled model-generated sea surface temperatures.
5) NOANVILO: Similar to NOANVIL, but using Q fluxes that were obtained by prescribing the coupled model-generated sea surface temperatures.
6) NOTAUFBO: Similar to NOTAUFB, but using Q fluxes that were obtained by prescribing the coupled model-generated sea surface temperatures.

The details of the physics used in each experiment are summarized in Table 1.

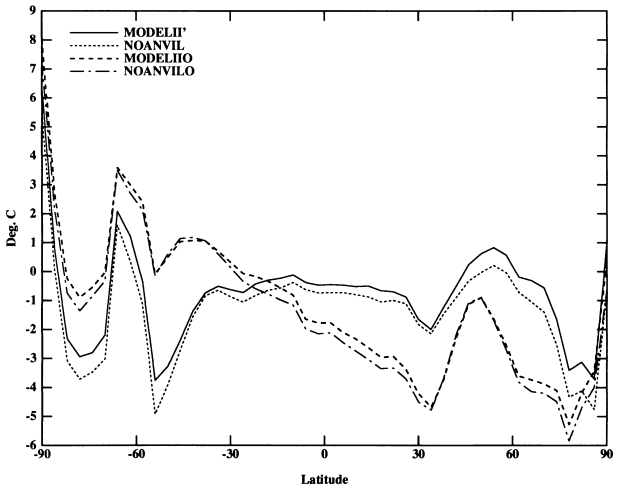

FIG. 2. Zonal mean and annual mean surface air temperature (°C) differences in the current climate between each of the simulations and the climatology of Legates and Willmott (1990).

3. Comparison of the controls

We are primarily concerned with how climate sensitivity differences due to different cloud parameterizations are affected by different SST distributions. Therefore, we show here only those current climate results that exhibit significant differences when the coupled model Q fluxes are substituted for the observed SST Q fluxes, that are directly related to cloud–radiation interaction, and that may help explain the differences in climate sensitivity. Differences due to changes in cloud parameterization among the prescribed SST Q-flux set of experiments (MODELII′, NOANVIL, NOTAUFB) are described in detail by Yao and Del Genio (1999).

It is logical first to see how different the sea surface temperatures of MODELIIO are from those of MODELII′ (Fig. 1). Their differences also represent the deviations of MODELIIO's simulation of sea surface temperature from observations. The ground temperature shown in Fig. 1 is identified as the sea surface temperature over the ocean area. It is quite clear that MODELIIO produces sea surface temperatures that are too warm in the southern oceans and too cold in the northern

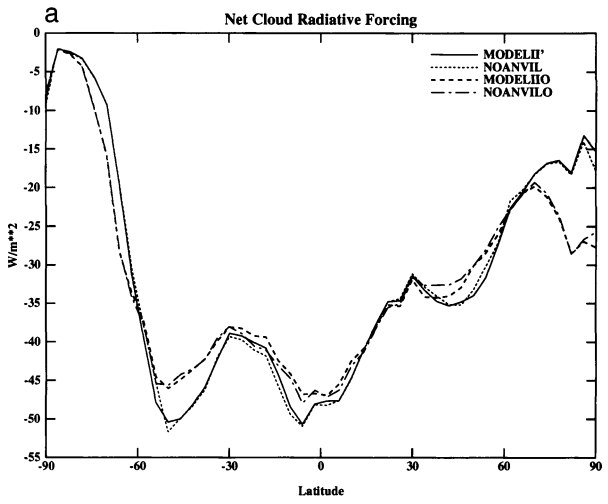

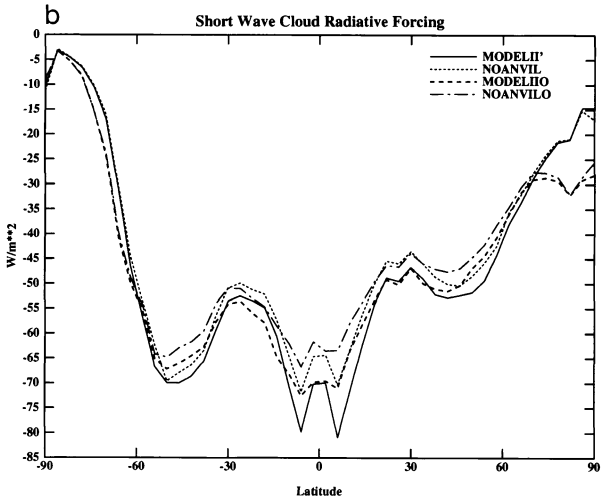

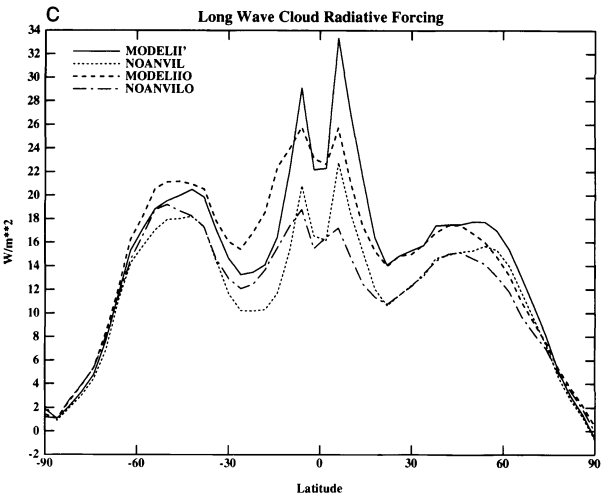

FIG. 3. As in Fig. 2, but for CRF (W m^{-2}): (a) net CRF, (b) shortwave CRF, and (c) longwave CRF.

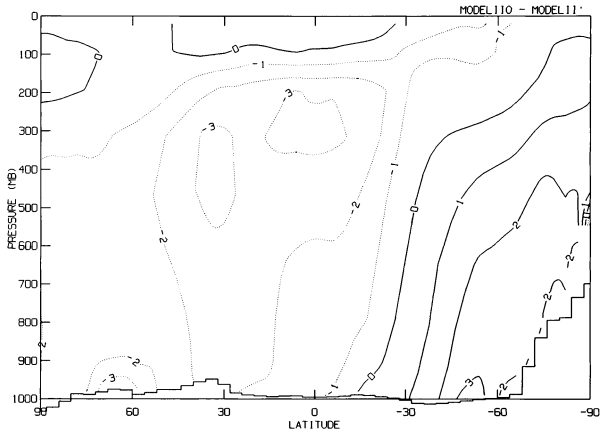

FIG. 4. Pressure–latitude cross section of temperature differences (°C) between MODELIIO and MODELII′.

oceans. The sea surface temperatures of MODELIIO are too warm over eastern oceans off the continental west coasts. It is not our purpose here to investigate the causes of these differences, but insufficient production of stratocumulus/stratus and inadequate ocean upwelling may contribute to warmer eastern oceans and the sea ice scheme may cause the differences in the polar/high latitudes.

Table 2 shows the annual mean and global mean values of current climate parameters. The surface air temperature (T_s) and ground uppermost layer temperature (T_g) of MODELIIO are 0.5°–0.6°C lower than those of MODELII′, suggesting that the coupled model run that was used to generate sea surface temperatures for MODELIIO has significant climate drift and may also not have reached final equilibrium yet (T_s increases 0.023°C yr^{-1} in the last 10 yr). However, since most coupled model experiments do not run long enough to reach equilibrium for practical reasons, our limitation of only integrating 50 yr is relevant to climate projections conducted by many AOGCMs (e.g., Russell et al. 1995), which start from the current state and actually include the drift that exists in the model. Note that due to the surface solar correction we apply, the planetary energy imbalances in Table 2 are not actually applied at the ocean surface, which can limit the extent of climate drifts. The lower T_g or T_s of MODELIIO itself certainly can cause some differences in climate sensitivity. The sea ice coverage of MODELII′ is 5.0%, which is slightly greater than 4.8% in the preliminary run when the observed sea surface temperatures were prescribed. The sea ice coverage of MODELIIO is smaller than that of MODELII′, apparantly due to the higher T_g that is simulated in the Southern Hemisphere.

Eliminating anvil clouds (NOANVIL and NOANVILO) tends to lower T_g or T_s in this model, despite not changing net cloud forcing (as we show later), because the atmosphere without detrained water is drier and loses heat from the surface more easily. Smaller amounts of middle and high clouds in NOANVIL and

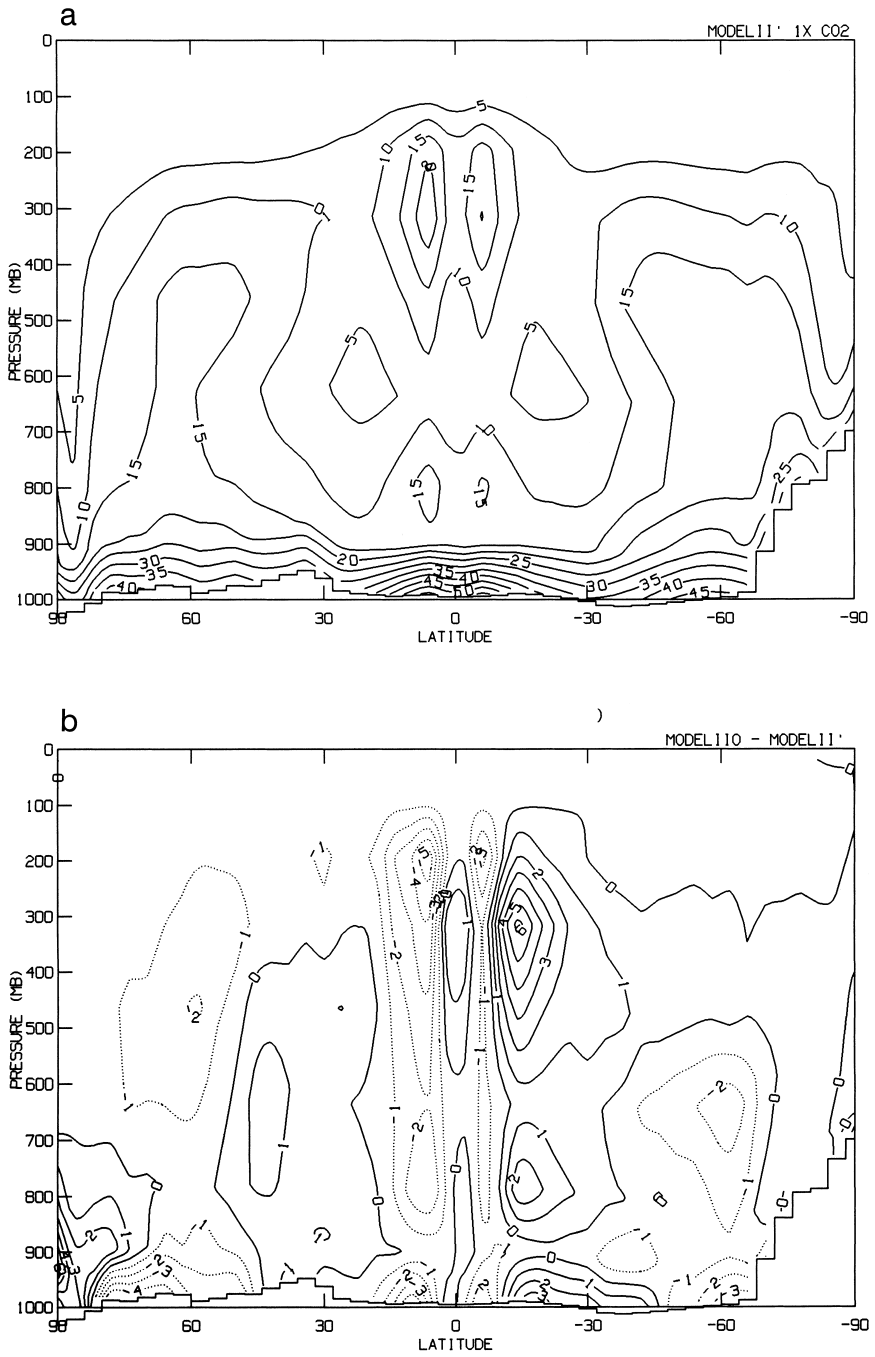

FIG. 5. As in Fig. 4, but for total cloud cover (%): (a) MODELII′ and (b) MODELIIO − MODELII′.

NOANVILO are certainly related to the omission of anvil clouds. The sea ice coverage of NOANVIL is 5.6%, which is consistent with its lower surface temperature.

Figure 2 shows the meridional distribution of T_s of the controls relative to observations. MODELII′ and NOANVIL are about 6 K warmer than the observed T_s at the South Pole, about 2 K colder elsewhere in both polar regions, too warm at both sea ice margins, and too cold in the poorly observed southern midlatitudes, but within 1 K at other latitudes, because here the implied ocean heat transports are defined to be consistent with observed sea surface temperatures. The larger differences in high latitudes are likely associated with snow/ice–albedo interaction, lapse rate, and dynamic transports in the atmosphere. The T_s of Legates and

TABLE 3. Changes of global mean and annual mean climate parameters. Here Q is the absorbed solar radiation, and F is the net longwave radiation. TOA is top of atmosphere. Cloud cover and albedo are in %; radiative and turbulent fluxes are in W m^{-2}.

	MODELII′	NOANVIL	MODELIIO	NOANVILO
T_s (°C)	4.11	4.93	3.02	2.78
T_g (°C)	3.99	4.79	2.90	2.67
Total cloud	−0.62	−0.79	0.22	0.27
Low cloud	−1.68	−1.75	−0.22	0.07
Middle cloud	−0.59	−0.09	−0.56	−0.69
High cloud	1.00	1.33	1.38	1.11
Cloud height (mb)	−10.00	−14.8	−9.4	−6.8
Planetary albedo	−0.65	−1.06	−0.11	−0.17
Ground albedo	−0.96	−1.24	−0.37	−0.37
Q at TOA	2.22	3.64	0.35	0.57
F at TOA	−2.36	−3.71	−0.38	−0.61
Net radiation at TOA	−0.14	−0.07	−0.03	−0.05
Q at surface	0.42	1.45	−1.17	−0.94
F at surface	3.73	4.50	3.84	3.83
Net radiation at surface	4.15	5.95	2.67	2.90
Net heat at surface	0.15	0.23	0.13	0.06
Latent heat flux	−6.19	−8.60	−4.62	−5.24
Sensible heat flux	1.89	2.52	1.96	2.31
Precipitation (mm day^{-1})	0.21	0.30	0.16	0.18
Ocean ice (%)	−2.31	−3.05	−0.68	−0.65
Lapse rate (°C km^{-1})	−0.15	−0.22	−0.09	−0.09
Precipitable water (mm)	7.54	9.16	5.61	4.87

Willmott (1990) may not be consistent with the data of SST applied in the model and can contribute to those differences. MODELIIO and NOANVILO, while showing similar features of meridional variation as in MODELII′ and NOANVIL, are generally warmer in the Southern Hemisphere and colder in the Northern Hemisphere as noted in Fig. 1, but the relatively well-simulated T_s between 30°S and 30°N in MODELII′ and NOANVIL deteriorates sharply in the coupled model. This is likely the main reason that the Q flux and dynamic ocean models produce different cloud feedbacks (see discussion in section 4). The T_s simulation of MODELIIO and NOANVILO increases the meridional temperature gradient in the Northern Hemisphere and decreases the meridional temperature gradient in the Southern Hemisphere, and this potentially can lead to different climate sensitivity between the two hemispheres (cf. Rind 1987, 1998).

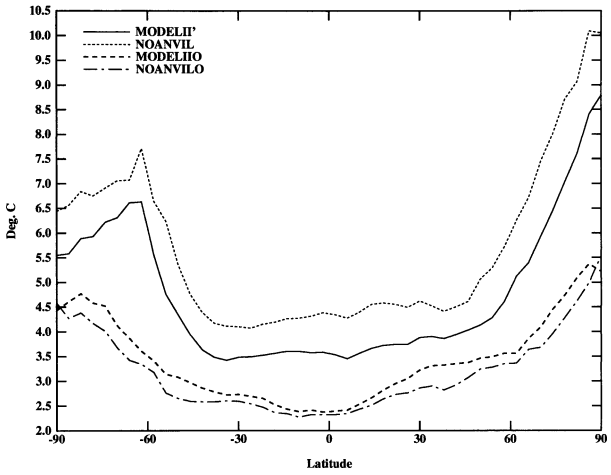

FIG. 6. Zonal mean and annual mean changes in surface air temperature (°C).

Figure 3 shows the meridional distribution of CRF of controls. All four experiments shown appear to produce similar magnitude and meridional distributions of net CRF, as well as of shortwave and longwave CRF, although the magnitude of shortwave and longwave CRF of the no-anvil cases are somewhat smaller outside the polar regions than the cases with anvil clouds. The similarity of CRF among the experiments does not clearly give any hints that may lead to different climate sensitivities.

To see differences in vertical structure between various experiments, we show several pressure–latitude cross sections in the following examples.

Figure 4 shows the pressure–latitude cross section of temperature differences between MODELIIO and MODELII′. The temperature distributions of the no-anvil cases are similar to those of the cases with anvil clouds, and are not shown. From Fig. 4, it is apparent that the colder temperature in the Northern Hemisphere and warmer temperature in the Southern Hemisphere in MODELIIO extend from the surface all the way to the upper troposphere with the maximum difference as high as 3°C.

Figure 5 shows pressure–latitude cross sections of total cloud cover of MODELII′ and the differences between MODELO and MODELII′. The total cloud distributions, as well as cloud water content distributions, of the no-anvil cases are similar to those of the cases with anvil clouds in the lower atmosphere, but the total cloud cover and cloud water content are much more reduced as expected in the upper troposphere, especially in the Tropics, when anvil clouds are eliminated (not

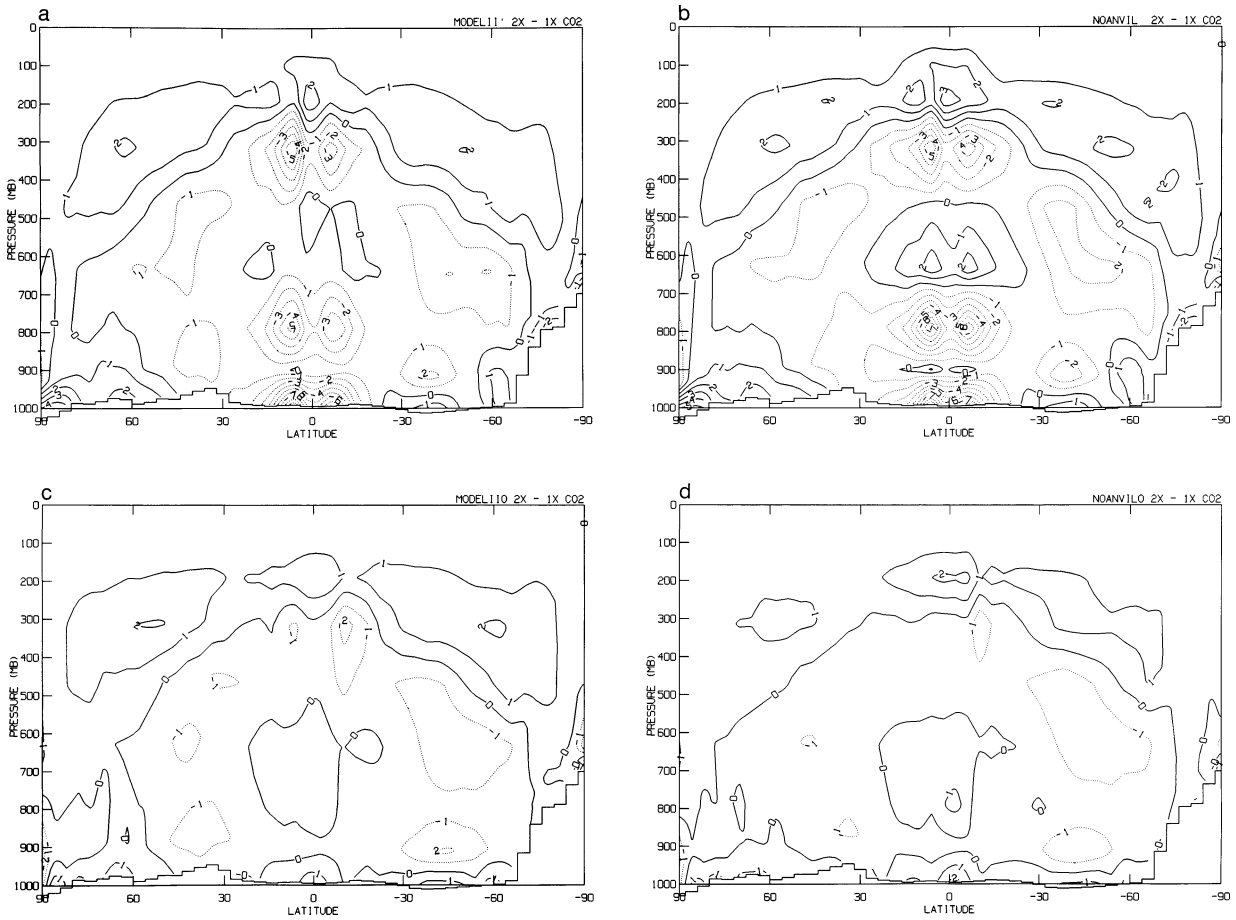

FIG. 7. Pressure–latitude cross sections of changes in total cloud cover (%): (a) MODELII′, (b) NOANVIL, (c) MODELIIO, and (d) NOANVILO.

shown here; cf. Fig. 5 and 6 in Yao and Del Genio 1999). From Fig. 5, the total cloud cover differences between MODELIIO and MODELII′ appear to be fairly complicated. In particular, the total cloud cover is more in the southern subtropics and less in the northern subtropics in MODELIIO versus MODELII′. A slight shift of the Hadley cell's position and a weaker Hadley cell (by 50%) in the Southern Hemisphere in MODELIIO (not shown) may contribute to these differences. The differences in the surface temperature simulations (see Fig. 1) can, of course, produce significant differences in the meridional circulation. The differences of low clouds are closely related to the relative humidity (not shown), which, in turn, is highly influenced by dynamics and SST. Low clouds near the sea ice margin in both hemispheres are less, and may contribute to that run having less sea ice, since more sunlight reaches the surface.

4. Climate changes due to doubling CO_2 and climate sensitivity analysis

The climate changes resulting from doubling CO_2 will be primarily discussed in terms of global means and zonal means to limit the discussion. Table 3 shows changes of annual mean and global mean climate parameters. The ΔT_s is 4.11°C in MODELII′, only slightly smaller than 4.2°C obtained by Hansen et al. (1984). The ΔT_s increases to 4.93°C in NOANVIL, suggesting that anvil clouds of large optical thickness reduce the climate sensitivity, as mentioned in Yao and Del Genio (1999). The ΔT_s for MODELIIO is 3.02°C; the reduced sensitivity is due both to reduced sea ice/snow–albedo feedback (based on changes in sea ice coverage and thus clear-sky solar fluxes, as we will discuss later) and reduced cloud cover feedback, the latter resulting mainly from reduced decreases of low clouds in the warmer climate. The ΔT_s for NOANVILO is 2.78°C, that is, the effect of removing anvils is opposite that for the case using the Q fluxes obtained by prescribing the observed sea surface temperatures. This occurs because the cooler tropical ocean of MODELIIO (see Figs. 1 and 2) produces thinner anvils whose longwave cloud forcing exceeds their shortwave impact; when these anvils are removed, there is only a weak negative impact on cloud water content and cloud forcing (see Fig. 8; Table 4). Results from NOTAUFB and NOTAUFBO (see Table

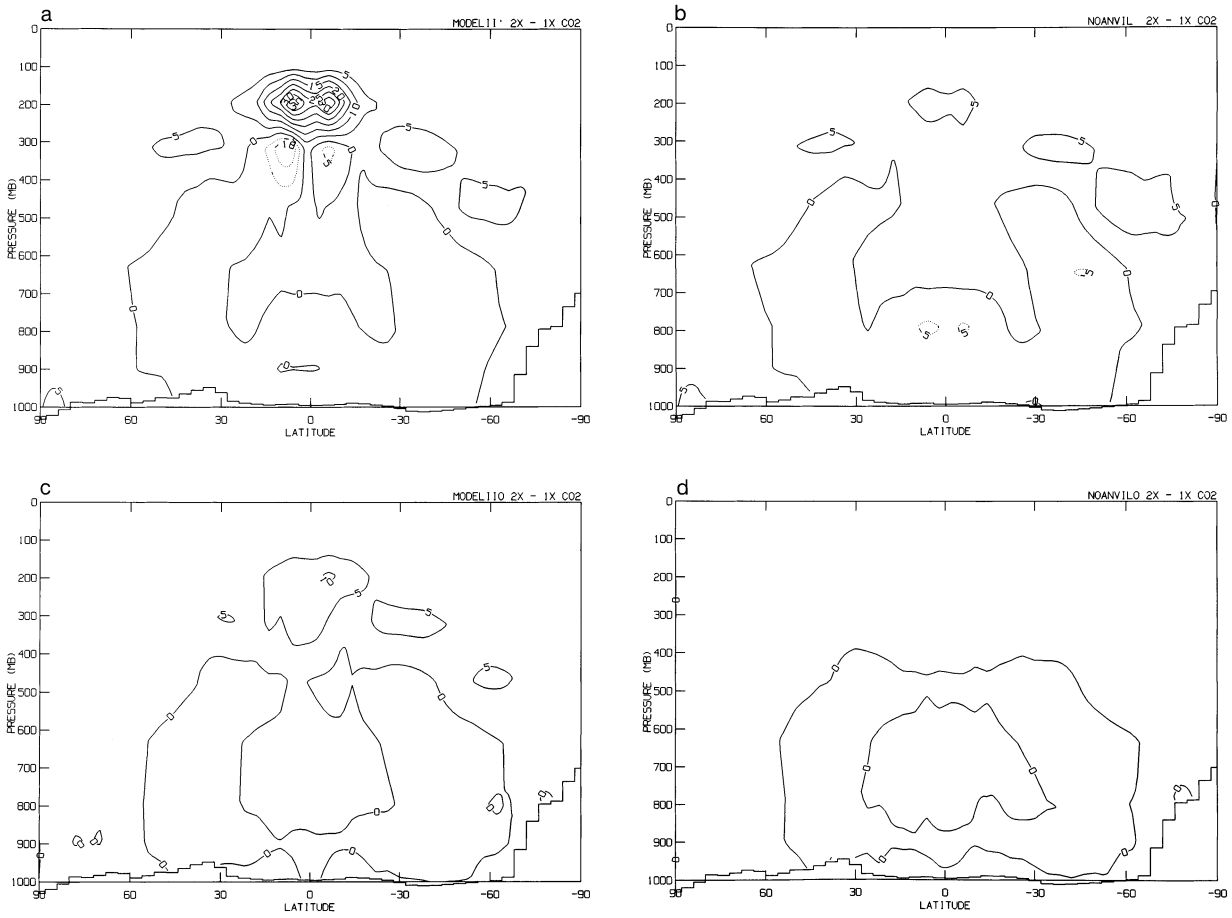

FIG. 8. As in Fig. 7, but for cloud water content (10^{-6} g g^{-1}): (a) MODELII′, (b) NOANVIL, (c) MODELIIO, and (d) NOANVILO.

4) both indicate that the cloud optical thickness feedback is positive as discussed in Yao and Del Genio (1999) and is not significantly affected by sea surface temperature distributions.

Figure 6 shows the meridional distributions of ΔT_s. The ΔT_s of NOANVIL is significantly higher than that of MODELII′, consistent with their global values. The ΔT_s increases generally toward the Poles, as obtained in other models (cf. Hansen et al. 1984; Wetherald and Manabe 1986), due to the snow/ice–albedo feedback and increases of lapse rate in the convectively stable higher latitudes (cf. Hansen et al. 1984), but ΔT_s of MODELII′ and NOANVIL show gradual decreases south of 60°S, probably due to reduced snow/ice–albedo feedback over the Antarctic.

To understand the reasons for different magnitudes and patterns of surface temperature changes in different experiments from the viewpoint of cloud feedbacks, we examine changes in cloud cover, cloud water content, and cloud radiative forcings. Figure 7 shows pressure–latitude cross sections of total cloud cover changes due to doubling CO_2. NOANVIL and MODELII′ show similar changes in total cloud cover, with increases in high clouds and decreases in low clouds in lower latitudes suggesting a positive feedback of cloud cover and height. Increases of low clouds in high latitudes explain why the cloud feedback is actually negative in high latitudes (see Fig. 9). NOANVILO and MODELIIO are similar in total cloud cover changes, with magnitude in NOANVILO being slightly larger, but increases of lower clouds through most latitudes effectively neutralize the positive feedback of high clouds. This occurs because increases in convection strength in the warmer climate are less dramatic in MODELIIO and NOANVILO due to their cooler tropical oceans (Fu et al. 1990). Thus, removal of boundary layer moisture by convection does not keep pace with the increased evaporation as the climate warms.

Figure 8 shows the cloud water content changes due to doubling CO_2. The sharp increases of cloud water in the upper tropical troposphere in MODELII′ versus NOANVIL indicate that anvil clouds of large cloud water content have a negative feedback effect in the warmer climate and serve to limit the increase of surface temperature, as discussed in Yao and Del Genio (1999). However, increases of cloud water content in the upper tropical troposphere are sharply reduced in MODELIIO, which actually changes the sign of the feedback asso-

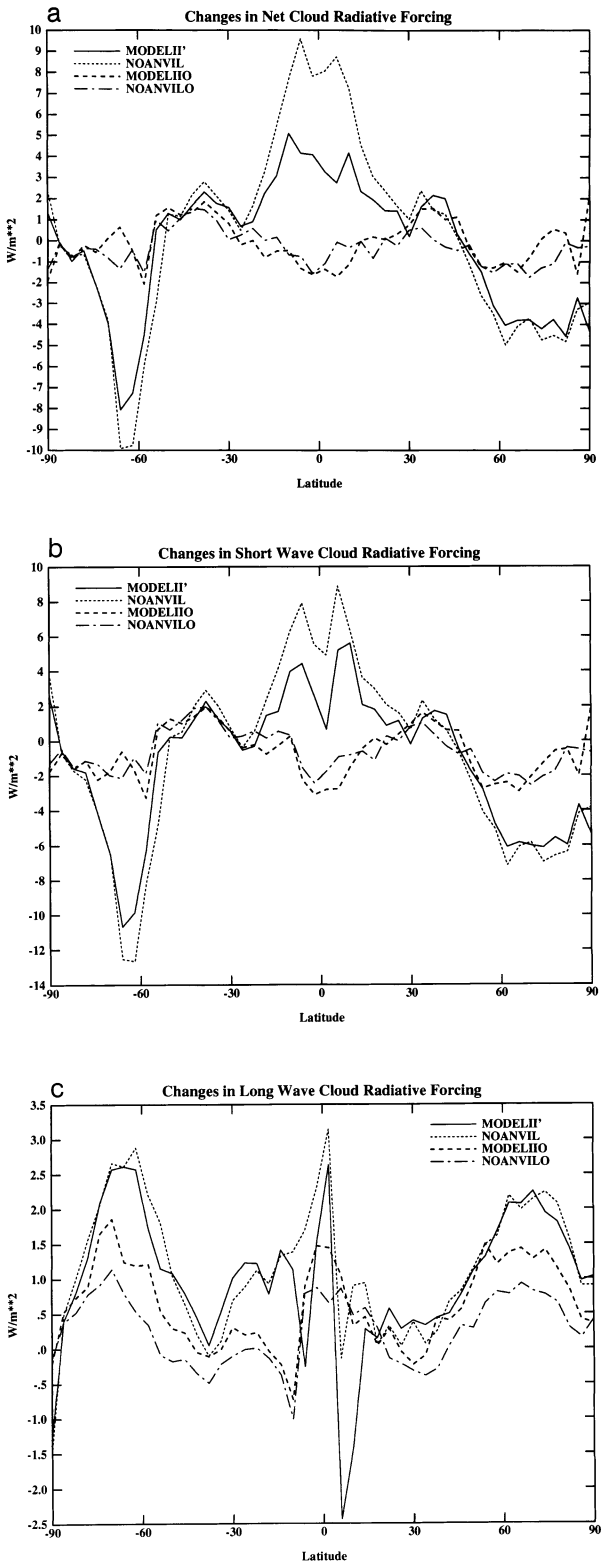

FIG. 9. As in Fig. 3, but for changes in CRF (W m^{-2}): (a) net CRF, (b) shortwave CRF, and (c) longwave CRF.

ciated with the cloud anvils. The smaller ΔT_s of MODELIIO versus MODELII′ is largely due to the negative cloud cover feedback and a smaller sea ice/snow–albedo feedback. Overall the cloud feedback is nearly neutral in MODELIIO versus a positive cloud feedback in MODELII′, as discussed below.

Investigating cloud radiative forcing and its changes is a common practice in the study of cloud feedbacks. Here, we use method 2 of Ramanathan et al. (1989). The details of formulation for our study were shown in Yao and Del Genio (1999). By computing

$$\lambda/\lambda_c = 1 + \Delta\text{CRF}/G, \tag{3}$$

one can determine the sign of the cloud feedback. Here $\lambda = \Delta T_s/G$ is a climate sensitivity parameter defined by Cess and Potter (1989), where $G = \Delta F - \Delta Q$, the radiative imbalance at the top of the atmosphere (TOA). Here Q and F represent the incoming solar radiation and outgoing longwave radiation at TOA. CRF = $(Q - Q_c) - (F - F_c)$, where Q_c and F_c are clear-sky Q and F, respectively. The λ_c is the clear-sky sensitivity parameter. For positive cloud feedback, $\lambda/\lambda_c > 1$; for negative cloud feedback, $\lambda/\lambda_c < 1$; when $\lambda/\lambda_c = 0$, the cloud feedback is neutral.

Table 4 shows the changes of total and clear-sky fluxes, CRF, λ, λ_c, and λ/λ_c along with ΔT_s for each of the experiments. Note first that the increase in clear-sky solar flux ΔQ_c is less than half as large in the set of experiments based on computed ocean SST Q fluxes as it is in the experiments using observed SST-based Q fluxes. This is indicative of the much weaker sea ice/snow–albedo feedback in the former runs, as mentioned earlier. For each pair of experiments with identical cloud parameterization but different SST, the difference of ΔQ_c is somewhat larger than the difference of $\Delta(\text{CRF})_{\text{sw}}$, though both are significant. The λ/λ_c indicates that the cloud feedback is positive in MODELII′, more positive in NOANVIL, near neutral in MODELIIO, slightly negative in NOANVILO, and negative in NOTAUFB and NOTAUFBO. The $\lambda/\lambda_c < 1$ both in NOTAUFB and NOTAUBFO proves that the positive cloud optical thickness feedback is robust to the differences in sea surface temperature in our model.

The meridional variations of ΔCRF (Fig. 9) show that for MODELII′ and NOANVIL, the cloud feedback is positive in low- and midlatitudes but negative in the polar regions; but for MODELIIO and NOANVILO, the cloud feedback is slightly negative even in low latitudes, with meridional variations being rather small. This is consistent with the generally smaller role played by changes in convection in runs with cooler ocean temperatures (Fig. 10). However, the changes of longwave radiative forcing in the four experiments shown (Fig. 9c) are mostly positive but with smaller magnitude in MODELIIO and NOANVILO. For cases of no optical thickness feedback, one can refer to Fig. 16 of Yao and Del Genio (1999).

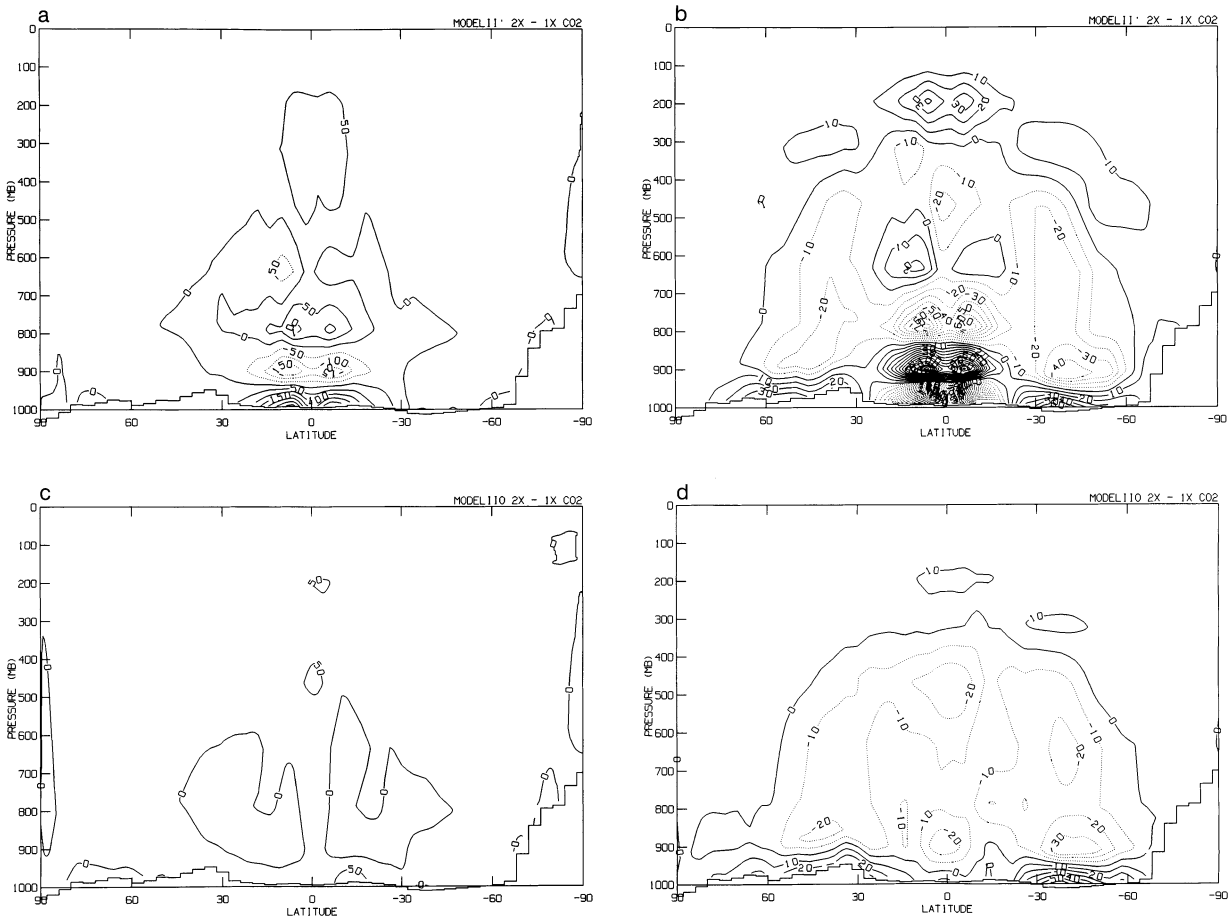

FIG. 10. As in Fig. 7, but for condensation heating (10^{13} W): (a) by moist convection in MODELII′, (b) by large-scale condensation in MODELII′, (c) by moist convection in MODELIIO, and (d) by large-scale condensation in MODELIIO.

5. Discussion and conclusions

We have conducted two sets of equilibrium doubled CO_2 experiments with the GISS GCM to study the effects on climate sensitivity of sea surface temperature: one set using the Q fluxes obtained by prescribing the observed sea surface temperatures (MODELII′), and the other set using the Q fluxes obtained by prescribing the simulated sea surface temperatures of a coupled model (MODELIIO).

The global and annual mean surface air temperature change obtained by MODELII′ is reduced from 4.11° to 3.02°C in MODELIIO. This reduced sensitivity, aside from reduced sea ice/snow–albedo feedback, is mainly due to the cloud feedback becoming nearly neutral in MODELIIO. The negative effect on climate sensitivity of anvil clouds of large optical thickness identified in Yao and Del Genio (1999) changes its sign in MODELIIO, primarily due to sharply reduced increases of

TABLE 4. Climate sensitivity and TOA radiation budget changes (W m^{-2}) for each of the experiments.

	MODELII′	NOANVIL	NOTAUFB	MODELIIO	NOANVILO	NOTAUFBO
ΔT_s (°C)	4.11	4.93	3.34	3.02	2.78	2.53
ΔQ	2.19	3.51	2.14	0.40	0.52	0.60
ΔF	2.41	3.89	2.46	0.51	0.63	0.64
ΔQ_c	2.04	2.65	1.93	0.95	0.88	0.85
ΔF_c	3.23	4.98	1.88	1.02	0.80	0.19
$\Delta(\text{CRF})_{sw}$	0.15	0.86	0.21	−0.55	−0.36	−0.70
$\Delta(\text{CRF})_{lw}$	0.82	1.08	−0.58	0.51	0.17	−0.25
ΔCRF	0.97	1.94	−0.37	−0.04	−0.18	−0.45
λ (°C m^2 W^{-1})	0.98	1.17	0.80	0.72	0.66	0.60
λ_c (°C m^2 W^{-1})	0.80	0.80	0.87	0.73	0.69	0.72
λ/λ_c	1.23	1.46	0.91	0.99	0.96	0.83

cloud water content in the tropical upper troposphere. However, the positive optical thickness feedback is still maintained in MODELIIO.

Our analysis indicates that the colder temperatures in the Tropics in MODELIIO and NOANVILO versus MODELII′ result in weaker deep convective activity and a more humid lower atmosphere in the warmer climate, which then eliminates the negative feedback of anvil clouds and sharply reduces the positive feedback of low clouds. Overall, the positive cloud feedback of MODELII′ is reduced to become nearly neutral in MODELIIO.

The actual sign of anvil cloud feedback is unknown. Lindzen et al. (2001) propose that it is strongly negative, based on inferred decreases in cloud cover with warming coupled with positive net forcing. Lin et al. (2001), on the other hand, using the Tropical Rainfall Measuring Mission (TRMM) satellite measurements over tropical oceans, suggest that the net anvil forcing is negative, so that a decrease in anvil cloud cover would produce a positive feedback. Del Genio and Kovari (2002) separate the temperature from the vertical velocity dependence in TRMM data and show that anvil cloud cover actually increases with warming. Thus, the feedback depends on the aggregate cloud forcing of optically thick and thin parts of convective systems.

The case we presented may be somewhat exaggerated, but its magnitude of difference makes it easier to identify its effects and provides an explanation. Nevertheless, the likelihood of changes in climate sensitivity in a coupled model because of poor simulation of sea surface temperature is clearly a reason for concern. Furthermore, climate sensitivity is also likely to undergo significant changes when the sea surface temperatures change in different ways, as in paleoclimate simulations (e.g., Rind 1998; Hewitt et al. 2001). Ye et al. (1998), for example, show that the atmospheric response to a prescribed cooling is not simply the mirror image of the response to a similar warming because of changes in the relative contribution of convection to the energy budget.

The underestimates of stratocumulus/stratus over eastern oceans, a common problem in GCMs (cf. Ma et al. 1996), may have some impact on climate sensitivity and cloud feedbacks. This should be a focus for future studies. Furthermore, a sea ice scheme that can simulate realistic sea ice distributions in dynamic ocean models is obviously a prerequisite for maintaining not only a realistic sea ice/snow–albedo feedback but a realistic cloud feedback as well.

Acknowledgments. We thank X. Jiang for providing guidance on setting up the coupled model run at GISS. This work was supported by the NASA Earth Sciences Modeling and Analysis Program, the NASA Tropical Rainfall Measuring Mission, and the DOE Atmospheric Radiation Measurement Program.

REFERENCES

Cess, R. D., and G. L. Potter, 1988: A methodology for understanding and intercomparing atmospheric climate feedback processes in general circulation models. *J. Geophys. Res.*, **93,** 8305–8314.

——, and Coauthors, 1990: Intercomparison and interpretation of climate feedback processes in 19 atmospheric general circulation models. *J. Geophys. Res.*, **95,** 16 601–16 615.

——, and Coauthors, 1996: Cloud feedback in atmospheric general circulation models: An update. *J. Geophys. Res.*, **101,** 12 791–12 794.

Del Genio, A. D., and M.-S. Yao, 1993: Efficient cumulus parameterization for long-term climate studies: The GISS scheme. *The Representation of Culumus Convection in Numeric Models. Meteor. Monogr.*, No. 46, Amer. Meteor. Soc., 181–184.

——, and W. Kovari, 2002: Climatic properties of tropical precipitating convection under varying environmental conditions. *J. Climate*, **15,** 2597–2615.

——, M.-S. Yao, W. Kovari, and K.-W. Lo, 1996: A prognostic cloud water parameterization for global climate models. *J. Climate*, **9,** 270–304.

Fu, R., A. D. Del Genio, and W. B. Rossow, 1990: Behavior of deep convective clouds in the tropical Pacific deduced from ISCCP radiances. *J. Climate*, **3,** 1129–1152.

Hansen, J., and L. D. Travis, 1974: Light scattering in planetary atmospheres. *Space Sci. Rev.*, **16,** 527–610.

——, G. Russell, D. Rind, P. Stone, A. Lacis, S. Lebedeff, R. Ruedy, and L. Travis, 1983: Efficient three-dimensional global models for climate studies: Models I and II. *Mon. Wea. Rev.*, **111,** 609–662.

——, A. Lacis, D. Rind, G. Russell, P. Stone, I. Fung, R. Ruedy, and J. Lerner, 1984: Climate sensitivity: Analysis of feedback mechanisms. *Climate Processes and Climate Sensitivity*, J. E. Hansen and T. Takahashi, Eds., Amer. Geophys. Union, 130–163.

——, and Coauthors, 1997: Forcings and chaos in interannual to decadal climate change. *J. Geophys. Res.*, **102,** 25 679–25 720.

Hewitt, C. D., C. A. Senior, and J. F. B. Mitchell, 2001: The impact of dynamic sea-ice on the climatology and climate sensitivity of a GCM: A study of past, present and future climates. *Climate Dyn.*, **17,** 655–668.

Large, W. G., G. Danabasoglu, S. C. Doney, and J. C. McWilliams, 1997: Sensitivity to surface forcing and boundary layer mixing in a global ocean model: Annual-mean climatology. *J. Phys. Oceanogr.*, **27,** 2418–2447.

Legates, D. R., and C. J. Willmott, 1990: Mean seasonal and spatial variability in global surface air temperature. *Theor. Appl. Climatol.*, **41,** 11–21.

Levitus, S., 1982: *Climatological Atlas of the World Ocean.* NOAA Prof. Paper 13, 173 pp. and 17 microfiche.

Lin, B., B. A. Wielicki, L. H. Chambers, Y. Hu, and K.-M. Xu, 2002: The iris hypothesis: A negative or positive cloud feedback? *J. Climate*, **15,** 3–7.

Lindzen, R., M.-D. Chou, and A. Hou, 2001: Does the earth have an adaptive infrared iris? *Bull. Amer. Meteor. Soc.*, **82,** 417–432.

Ma, C.-C., C. R. Mechoso, A. W. Robertson, and A. Arakawa, 1996: Peruvian stratus clouds and the tropical Pacific circulation: A coupled ocean–atmosphere GCM study. *J. Climate*, **9,** 1635–1645.

Mechoso, C. R., and Coauthors, 1995: The seasonal cycle over the tropical Pacific in coupled ocean–atmosphere general circulation models. *Mon. Wea. Rev.*, **123,** 2825–2838.

Mitchell, J. F. B., C. A. Senior, and W. J. Ingram, 1989: CO_2 and climate: A missing feedback? *Nature*, **341,** 132–134.

Ramanathan, V., B. R. Barkstrom, and E. F. Harrison, 1989: Climate and the earth's radiation budget. *Phys. Today*, **42,** 22–32.

Rind, D., 1987: The doubled CO_2 climate: Impact of the sea surface temperature gradient. *J. Atmos. Sci.*, **44,** 3235–3268.

——, 1998: Latitudinal temperature gradients and climate change. *J. Geophys. Res.*, **103,** 5943–5971.

Russell, G. L., J. R. Miller, and D. Rind, 1995: A coupled atmosphere–

ocean model for transient climate change studies. *Atmos.–Ocean,* **33,** 683–730.
Senior, C. A., and J. F. B. Mitchell, 1993: Carbon dioxide and climate: The impact of cloud parameterization. *J. Climate,* **6,** 393–418.
Sundqvist, H., E. Berge, and J. E. Kristjansson, 1989: Condensation and cloud parameterization studies with a mesoscale numerical weather prediction model. *Mon. Wea. Rev.,* **117,** 1641–1657.
Wetherald, R. T., and S. Manabe, 1986: An investigation of cloud cover change in response to thermal forcing. *Climatic Change,* **8,** 5–23.
Yao, M.-S., and A. D. Del Genio, 1989: Effects of cumulus entrainment and multiple cloud types on a January global climate model simulation. *J. Climate,* **2,** 850–863.
——, and ——, 1999: Effects of cloud parameterization on the simulation of climate changes in the GISS GCM. *J. Climate,* **12,** 761–779.
Ye, B., A. D. Del Genio, and K. K.-W. Lo, 1998: CAPE variations in the current climate and in a climate change. *J. Climate,* **11,** 1997–2015.